J Low Temp Phys (2008) 151: 173–179
DOI 10.1007/s10909-007-9615-3

# Sensitivity Measurements of a Transition-Edge Hot-Electron Microbolometer for Millimeter-Wave Astrophysical Observations

**E.M. Barrentine · P.T. Timbie · T.R. Stevenson · S. Ali · J.A. Chervenak · E. Wollack · S.H. Moseley · C.A. Allen · W.T. Hseih · T.M. Miller · D.J. Benford · A.D. Brown**

Received: 22 July 2007 / Accepted: 15 September 2007 / Published online: 17 January 2008


**Abstract** Future experiments to probe the Cosmic Microwave Background (CMB) polarization will need arrays of 1000s of sensitive bolometers. We are developing a Transition-edge Hot-electron Microbolometer (THM) to fill this need. This small-volume bolometer consists of a superconducting bilayer Transition-Edge Sensor (TES) with a thin-film absorber. Unlike traditional monolithic bolometers which make use of micromachined structures, the THM employs the decoupling between electrons and phonons at milliKelvin temperatures to provide thermal isolation. The devices are fabricated photolithographically and are easily integrated with antennas via microstrip transmission lines, and with SQUID readouts. We present the results of noise, responsivity, and thermal conductance measurements in which electrical power is dissipated in the absorber, and confirm a thermal model for a test THM with a Mo/Au TES and Bi/Au absorber.

**Keywords** Microbolometers · Transition-edge sensors · Cosmic microwave background · Millimeter waves · Hot-electron effect · Transition-edge hot-electron microbolometer

**PACS** 07.57.Kp

E.M. Barrentine (✉) · P.T. Timbie
University of Wisconsin-Madison, Madison, WI 53706, USA
e-mail: barrentine@wisc.edu

T.R. Stevenson · J.A. Chervenak · E. Wollack · S.H. Moseley · C.A. Allen · W.T. Hseih · T.M. Miller · D.J. Benford · A.D. Brown
NASA Goddard Space Flight Center, Greenbelt, MD 20771, USA

S. Ali
Lawrence Livermore National Laboratory, Livermore, CA 94550, USA

## 1 Introduction

The 2.7 K Cosmic Microwave Background (CMB) signal, which peaks at ∼150 GHz (∼2 mm), tells us about the conditions of the early universe at the time of recombination, and indirectly, about even earlier conditions, during the inflation era. A B-mode polarization anisotropy is expected to exist in the CMB at the 0.1 μK level and the detection of such a signal would confirm one of the key predictions of inflation, gravitational waves [1].

To detect B-mode polarization, arrays of thousands of photon-noise-limited detectors are necessary. One of the most promising technologies for large detector arrays includes planar antenna-coupled bolometers with TES thermometers read out by SQUIDs [2]. The THM is such a bolometer, which makes use of the strong hot-electron effect at milliKelvin temperatures for thermal isolation. It is similar to other hot-electron designs, [3] but includes a separate absorber structure for separate impedance matching to the antenna. An array of optimized THMs could reach the sensitivity level needed to detect B-modes.

As a first step towards understanding and optimizing this detector for CMB observations, we report the results of current-voltage (I-V), thermal conductance, responsivity and noise measurements of a test THM. We have developed a thermal model for this test device that confirms our understanding of the electron-phonon and electron-electron thermal properties of the THM.

## 2 THM Design and Thermal Models

The THM consists of a thin-film metal absorber overlapping a superconducting bilayer TES (Fig. 1). The absorber forms the termination of a superconducting microstripline that carries RF power from an antenna. For testing, the absorber can also be heated by passing DC current along the line. When power is deposited in the absorber, Andreev reflection [4] at the boundary between the normal absorber and superconducting microstrip prevents thermal power from leaving the absorber through the lines. Power is transmitted thermally along the absorber and to the TES via the electron-electron (e-e) Wiedemann-Franz conductance. The coupling between electrons and phonons (e-p) at milliKelvin temperatures within the small-volume of the

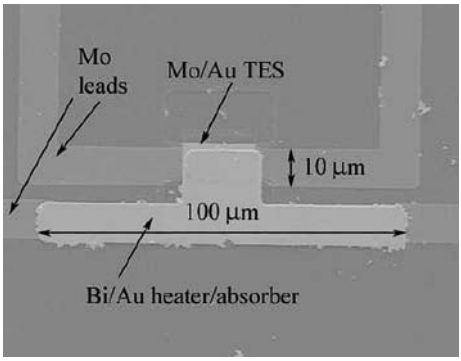


**Fig. 1** SEM image showing the THM test device components and their dimensions. The absorber Bi layer is 500 nm under a 190 nm Au layer. The TES is 40 nm Mo under a 150 nm Au layer

THM is weak. In an optimized THM the electrons in the absorber and TES are in thermal equilibrium and the hot-electron effect provides the thermal isolation for the bolometer. (i.e. $G_{e\text{-}e} > G_{e\text{-}p}$). The measurements of the thermal properties of the test device presented here will be used to optimize the design of future THMs.

Electrically, the TES is voltage-biased via a bias current to a shunt resistor ($R_s \ll R_{TES}$) in parallel with the TES, which provides negative electrothermal feedback to keep the TES in the transition region [5]. The output of the SQUID (with feedback) is proportional to the TES current, which is directly proportional to the incoming power via a responsivity, S [A/W].

Below we detail the design and measurements of a test THM and briefly introduce two thermal models for this device which incorporate the hot-electron behavior. In both thermal models, due to the small size, the heat capacity of the absorber and TES are assumed to be negligible. Although not shown here in detail, we have followed the matrix method [6, 7] to predict responsivity, and the amplifier, thermal and Johnson noise contributions for both thermal models for comparison to measurements of the test THM.

### 2.1 The Test Device

The THM test device consists of a thin Bi/Au absorber and bilayer Mo/Au TES (Fig. 1). For these tests the microstrip line is replaced by Mo leads attached to the absorber. These allow direct heating of the absorber by small applied DC currents. The TES transitions at 310–317 mK and has a normal resistance of 0.32 Ω. The absorber has a resistance of 17 Ω. Fabrication details and previous measurements of this test device can be found in the literature [8, 9].

### 2.2 Two Thermal Models

Electron-phonon conductance is given by $G_{e-p}(T) = 5V\Sigma T$ [4] where V is the volume and Σ is a material-dependent constant [10]. In the thermal model for an ideal THM, the e-e conductance along the length of the absorber is much larger than the

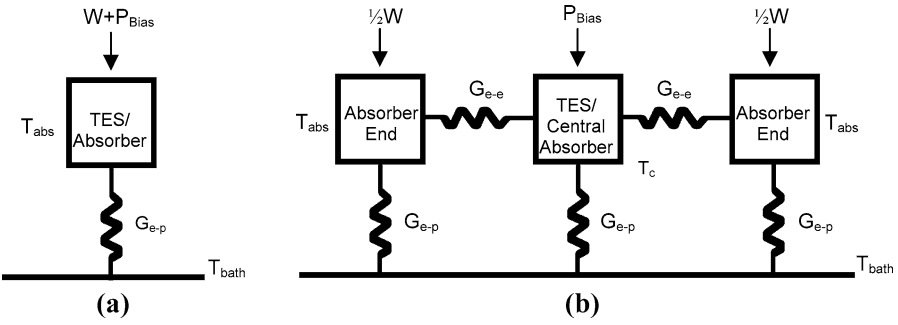


**Fig. 2** (**a**) Thermal model for an ideal THM. $W$ is power incident on the absorber, $P_{Bias}$ is Joule power due to the voltage bias of the TES, $T_c$ is the operating temperature for the TES, and $T_{bath}$ is the cold stage temperature. (**b**) Thermal model for a thermally disconnected THM. The ends of the absorber are at temperature $T_{abs}$, while the TES and the central portion of the absorber nearby the TES are at $T_c$

e-p conductance between the absorber and substrate. In this case we can model the detector as shown in Fig. 2a. The Wiedemann-Franz conductance along the absorber is given by $G_{e-e}(T, R) = L_0 T/R$ [11]. Here $L = 2.44 \times 10^{-8}$ W Ω/K$^2$ is the Lorenz number. In the second model, the e-e conductance is comparable to the weak e-p conductance and the ends of the absorber become thermally isolated from the TES and central portion of the absorber as shown in Fig. 2b. In this thermally "disconnected" model, some fraction of the incident power, W, bypasses the TES, leading to a reduction in sensitivity.

## 3 Measurements & Results

### 3.1 Test Setup

To measure the characteristics of the THM "in the dark", the test device was placed within a Nb can to shield stray magnetic fields, and was heat sunk to a cold stage cooled to 180–300 mK using a shielded ADR. The TES was placed in parallel with a shunt resistor with resistance, $R_S = 25$ mΩ, and was read out by a NIST 2-stage SQUID with mutual inductance M ∼ 190 pH.

### 3.2 I-V Measurements

The I-V characteristics of the TES were measured by applying an AC bias current to the TES bias circuit and observing the SQUID response. In Fig. 3 the I-V curves for the TES are shown at several cold stage temperatures. With $T < T_c$, at low TES bias-voltage, the TES remains in the superconducting regime. As the TES voltage and current increase the TES transitions to the normal linear regime. In the transition region the Joule power dissipation ($P_{Bias} = IV_{Bias}$) is constant since TES temperature is approximately constant in the transition and constant bias power is required to maintain the TES at a fixed temperature above the cold stage. This accounts for the negative slope of the I-V curve in the transition. As the cold stage temperature approaches $T_c$, the transition current decreases and the I-V curve approaches the normal linear regime. The I-V curves map out the TES bias points in the transition. Possible bias points for this test device range from ∼0.2 μV–3 μV.

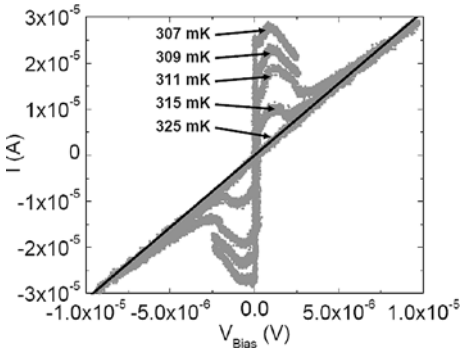


**Fig. 3** I-V curves at different cold stage temperatures. The *solid black line* indicates $R_{TES} = 0.32$ Ω

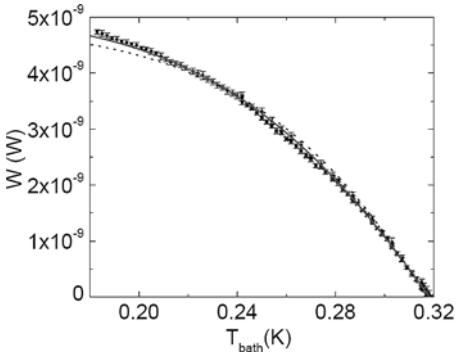


**Fig. 4** W vs $T_{bath}$ fit to the disconnected (*solid line*) and ideal (*dashed line*) models

**Table 1** $\Sigma_{Bi}$, $\Sigma_{Au}$ & thermal conductances (at 310 mK) resulting from fits to W vs. $T_{bath}$ (Fig. 4) for the disconnected and ideal models. For comparison, literature values are also shown. (For $G_{e\text{-}e}$, R = 17 Ω)

| | $\Sigma_{Au}$ [W/m$^3$K$^5$] | $\Sigma_{Bi}$ [W/m$^3$K$^5$] | $G_{e\text{-}pabs}$ [W/K] | $G_{e\text{-}pTES}$ [W/K] | $G_{e\text{-}e}$ [W/K] |
|---|---|---|---|---|---|
| Ideal | $6.5–6.9 \times 10^9$ | $2.4–1.2 \times 10^8$ | $6.1 \times 10^{-8}$ | $9.0–9.6 \times 10^{-9}$ | $4.5 \times 10^{-10}$ |
| Disconnected | $2.2–2.6 \times 10^9$ | $2.4–1.2 \times 10^8$ | $2.5 \times 10^{-8}$ | $3.1–3.6 \times 10^{-9}$ | $4.5 \times 10^{-10}$ |
| Literature [12, 13] | $3.3–5.7 \times 10^9$ | $2.4 \times 10^8$ | $3.4–5.4 \times 10^{-8}$ | $4.6–7.9 \times 10^{-9}$ | $4.5 \times 10^{-10}$ |

### 3.3 W vs. $T_{bath}$ & Thermal Conductance Measurements

To determine the thermal conductance of the test device, measurements were made of the amount of Joule power dissipation in the absorber, W, required to maintain the TES at $T_c$ as a function of the cold stage temperature. This was done by allowing the cold stage temperature to gradually rise from 180 mK to 320 mK and applying a DC current to the absorber while monitoring the I-V curve. A plot of W vs. $T_{bath}$ fitted to the two thermal models is shown in Fig. 4. The disconnected model provides the best fit to the temperature dependence of the power dissipation. The fitted e-p Σ values and conductances for both models are listed in Table 1. The disconnected model fits to Σ values only slightly lower than literature values [12, 13]. In all cases the e-p conductance is substantially greater than the e-e conductance along the absorber, further supporting a disconnected model for this test device.

### 3.4 Responsivity Measurements

The THM responsivity was measured by passing a small AC current through the absorber and using a lock-in amplifier to read out the AC SQUID response, while DC voltage-biasing the TES and regulating the cold stage temperature. Table 2 lists the measured responsivity of the THM for one TES voltage bias, $V_{Bias}$, and cold stage temperature, $T_{bath}$. For $W \geq 3.5 \times 10^{-10}$ W the response becomes non-linear. The measured responsivities agree within 10% to the predicted disconnected thermal model responsivities with literature [12, 13], and fit Σ values. The measured responsivities only agree within 50% to the ideal model.

**Table 2** Measured and predicted responsivity for both thermal models with fit and literature Σ values (Table 1) for $W \leq 3.5 \times 10^{-10}$ W

| $T_{bath}$ [mK] | $V_{Bias}$ [μV] | Measured S [A/W] | Disconnected | | Ideal S [A/W] |
|---|---|---|---|---|---|
| | | | Fit S [A/W] | Literature S [A/W] | |
| 311 | 1 | $3.1 \times 10^4$ | $2.9 \times 10^4$ | $2.9–5.5 \times 10^4$ | $4.5–6.9 \times 10^4$ |

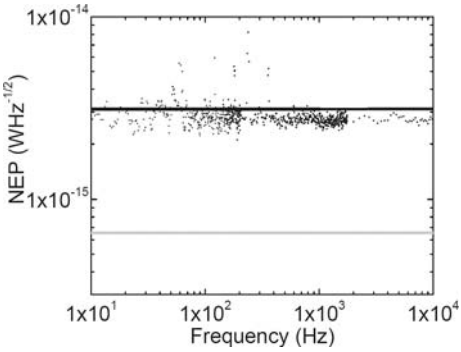


**Fig. 5** NEP measurement at $T_{bath} = 311$ mK for $V_{Bias} = 1$ μV. Plotted are predicted noise levels for SQUID, Johnson and thermal noise contributions for the disconnected (*black line*) and ideal (*gray line*) models for fit Σ values (Table 1)

### 3.5 Noise Measurements

The measured NEP of the THM at one TES bias is shown in Fig. 5. For comparison, the predicted NEPs for this test device for both thermal models are also shown. For these predictions we have assumed a radiative limit for the thermal noise contributions [14]. We measure $NEP \approx 3 \times 10^{-15}$ W Hz$^{-1/2}$ at various TES biases. The disconnected model provides a good match to the noise measurements. The ideal model does not adequately account for the noise. The noise of this device is still well above photon-noise levels. Under ground based observing conditions operating at 100 GHz with 20% bandwidth we calculate $NEP_{photon} \approx 3 \times 10^{-17}$ W Hz$^{-1/2}$. The peaks in the noise spectrum at low frequencies are believed to be due to external noise sources which can be minimized with further shielding.

## 4 Discussion

Based on the measurements of this first test device we have designed a new THM which meets photon-noise-limited levels and conforms to the ideal thermal model. This device will include a 20 Ω microstripline terminated by a 20 Ω absorber. Under the ground-based observing conditions assumed above we have applied an optimization scheme to the THM dimensions utilizing the confirmed Au and Bi Σ values and requiring $NEP_{detector} < NEP_{photon}$ and $G_{e\text{-}e} > G_{e\text{-}p}$. The result of this optimization is a new THM design consisting of a 4 μm × 7 μm absorber with 650 nm Bi overlapping a 3 μm × 3 μm TES with 40 nm Mo under a 150 nm Au layer.

## 5 Conclusions

The results of W vs. $T_{bath}$, conductance, responsivity & noise measurements for this THM test device are fit well by a thermal model in which the internal thermal conductance ($G_{e\text{-}e}$) of the THM is less than the conductance to the substrate ($G_{e\text{-}p}$). These results also agree with literature values for the e-p conductance of Au and Bi. To reach phonon noise-limited sensitivity levels in future devices we plan to decrease the THM area by two orders of magnitude and optimize the relative dimensions of the absorber and TES to operate within the ideal thermal model for this detector.

**Acknowledgements** We would like to thank Dan McCammon and Mark Lindeman for their helpful discussions and Kent Irwin for providing the SQUID readouts. EB would like to thank the Wisconsin Space Grant Consortium and the NASA-Goddard Graduate Student Research Program for support.

## References

1. W. Hu, S. Dodelson, Annu. Rev. Astron. Astrophys. **40**, 171 (2002)
2. Task Force on CMB Research, Final Report, http://www.nsf.gov/mps/ast/tfcr.jsp (2005)
3. B.S. Karasik, B. Delaet, W.R. McGrath, J. Wei, M.E. Gershenson, A.V. Sergeev, IEEE Trans. Appl. Superconduct. **13**, 188 (2003)
4. A.F. Andreev, Sov. Phys. JETP **19**, 1228 (1964)
5. K.D. Irwin, Appl. Phys. Lett. **66**, 1998 (1995)
6. M. Lindeman, Ph.D. Thesis, University of California, Davis (2000)
7. E. Figueroa-Feliciano, Ph.D. Thesis, Stanford University (2001)
8. S. Ali, L.D. Cooley, D. McCammon, K. Nelms, J. Peck, D. Prober, D. Swetz, P. Timbie, D. van der Weide, IEEE Trans. Appl. Superconduct. **13**, 184 (2003)
9. S. Ali, P.T. Timbie, S. Malu, D. McCammon, K.L. Nelms, R. Pathak, D. van der Weide, C.A. Allen, J. Abrahams, J. Chervenak, W.T. Hseih, T.M. Miller, S.H. Moseley, T.R. Stevenson, E. Wollack, Proc. SPIE Int. Soc. Opt. Eng. **5498**, 381 (2004)
10. F.C. Wellstood, C. Urbina, J. Clarke, Appl. Phys. Lett. **54**, 2599 (1989)
11. F. Pobell, *Matter and Methods at Low Temperature*, 2nd edn. (Springer, Berlin, 1996), p. 64
12. F. Pierre, A.B. Gougam, A. Anthore, H. Pothier, D. Esteve, N. Birge, Phys. Rev. B **68**, 085413 (2003)
13. S.I. Dorozhkin, F. Lell, W. Schoepe, Solid State Commun. **60**, 245 (1986)
14. W.S. Boyle, K.F. Rodgers, J. Opt. Soc. Am. **49**, 66 (1959)